

Local and Nonlocal Strain Rate Fields and Vorticity Alignment in Turbulent Flows

Peter E. Hamlington^{1*}, Jörg Schumacher^{2†}, and Werner J. A. Dahm^{1‡}

¹ *Laboratory for Turbulence & Combustion (LTC), Department of Aerospace Engineering,
The University of Michigan, Ann Arbor, MI 48109-2140, USA*

² *Department of Mechanical Engineering, Technische Universität Ilmenau, D-98684 Ilmenau, Germany*

(Dated: October 25, 2018)

Local and nonlocal contributions to the total strain rate tensor S_{ij} at any point \mathbf{x} in a flow are formulated from an expansion of the vorticity field in a local spherical neighborhood of radius R centered on \mathbf{x} . The resulting exact expression allows the nonlocal (background) strain rate tensor $S_{ij}^B(\mathbf{x})$ to be obtained from $S_{ij}(\mathbf{x})$. In turbulent flows, where the vorticity naturally concentrates into relatively compact structures, this allows the local alignment of vorticity with the most extensional principal axis of the background strain rate tensor to be evaluated. In the vicinity of any vortical structure, the required radius R and corresponding order n to which the expansion must be carried are determined by the viscous lengthscale λ_ν . We demonstrate the convergence to the background strain rate field with increasing R and n for an equilibrium Burgers vortex, and show that this resolves the anomalous alignment of vorticity with the intermediate eigenvector of the total strain rate tensor. We then evaluate the background strain field $S_{ij}^B(\mathbf{x})$ in DNS of homogeneous isotropic turbulence where, even for the limited R and n corresponding to the truncated series expansion, the results show an increase in the expected equilibrium alignment of vorticity with the most extensional principal axis of the background strain rate tensor.

PACS numbers: 47.27.-i, 47.32.C-, 47.27.De

I. INTRODUCTION

Vortex stretching is the basic mechanism by which kinetic energy is transferred from larger to smaller scales in three-dimensional turbulent flows [1, 2, 3, 4]. An understanding of how vortical structures are stretched by the strain rate field $S_{ij}(\mathbf{x})$ is thus essential to any description of the energetics of such flows. Over the last two decades, direct numerical simulations (DNS) [5, 6, 7] and experimental studies [8, 9, 10, 11, 12] of the fine-scale structure of turbulence have revealed a preferred alignment of the vorticity with the intermediate eigenvector of the strain rate tensor. This result has been widely regarded as surprising. Indeed the individual components of the inviscid vorticity transport equation, in a Lagrangian frame that remains aligned with the eigenvectors of the strain rate tensor, are simply

$$\frac{D\omega_1}{Dt} = s_1\omega_1, \quad \frac{D\omega_2}{Dt} = s_2\omega_2, \quad \frac{D\omega_3}{Dt} = s_3\omega_3, \quad (1)$$

where s_1 , s_2 and s_3 are the eigenvalues of S_{ij} . For incompressible flow, $s_1 + s_2 + s_3 \equiv 0$, and then denoting $s_1 \geq s_2 \geq s_3$ requires $s_1 \geq 0$ and $s_3 \leq 0$. As a consequence, (1) would predict alignment of the vorticity with the eigenvector corresponding to the most extensional principal strain rate s_1 . Yet DNS and experimental studies have clearly shown that the vorticity instead is aligned with the eigenvector corresponding to the *intermediate* principal strain rate s_2 .

A key to understanding this result is that, owing to the competition between strain and diffusion, the vorticity in turbulent flows naturally forms into concentrated vortical structures. It has been noted, for example in Refs. [7, 13, 14], that the anomalous alignment of the vorticity with the strain rate tensor $S_{ij}(\mathbf{x})$ might be explained by separating the local self-induced strain rate field created by the vortical structures themselves from the background strain field in which these structures reside. The total strain rate tensor is thus split into

$$S_{ij}(\mathbf{x}) = S_{ij}^R(\mathbf{x}) + S_{ij}^B(\mathbf{x}), \quad (2)$$

where S_{ij}^R is the *local* strain rate induced by a vortical structure in its neighboring vicinity, and S_{ij}^B is the *non-local* background strain rate induced in the vicinity of the structure by all the remaining vorticity. The vortical structure would then be expected to align with the principal axis corresponding to the most extensional eigenvalue of the background strain rate tensor $S_{ij}^B(\mathbf{x})$.

In the following, we extend this idea and suggest a systematic expansion of the total strain rate field $S_{ij}(\mathbf{x})$ that allows the background strain rate field $S_{ij}^B(\mathbf{x})$ to be extracted. Our approach is based on an expansion of the vorticity over a local spherical region of radius R centered at any point \mathbf{x} . This leads to an exact operator that provides direct access to the background strain rate field. The operator is tested for the case of a Burgers vortex, where it is shown that the local self-induced strain field produced by the vortex can be successfully removed, and the underlying background strain field can be increasingly recovered as higher order terms are retained in the expansion. The anomalous alignment of the vorticity with respect to the eigenvectors of the total strain field is shown in that case to follow from a local switch-

*email: peterha@umich.edu (corresponding author)

†email: joerg.schumacher@tu-ilmenau.de

‡email: wdahm@umich.edu

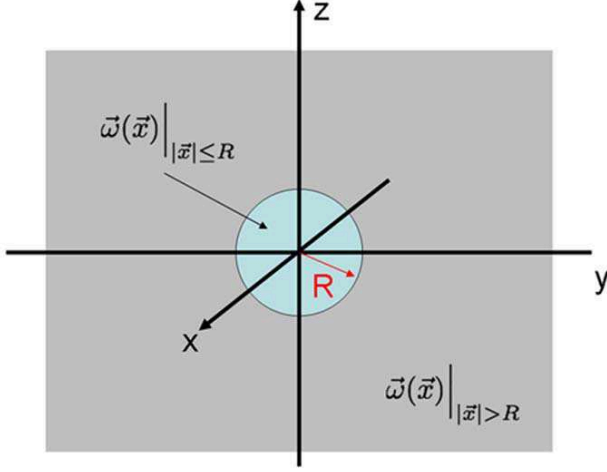


FIG. 1: Decomposition of the vorticity field in the vicinity of any point \mathbf{x} into local and nonlocal parts; the Biot-Savart integral in (8) over each part gives the local and nonlocal (background) contributions to the total strain rate tensor S_{ij} at \mathbf{x} .

ing of the principal strain axes when the vortex becomes sufficiently strong relative to the background strain. Finally, the operator is applied to obtain initial insights into the background strain $S_{ij}^B(\mathbf{x})$ in DNS of homogeneous isotropic turbulence, and used to compare the vorticity alignment with the eigenvectors of the total strain field and of this background strain field.

II. THE BACKGROUND STRAIN FIELD

The velocity \mathbf{u} at any point \mathbf{x} induced by the vorticity field $\boldsymbol{\omega}(\mathbf{x})$ is given by the Biot-Savart integral

$$\mathbf{u}(\mathbf{x}) = \frac{1}{4\pi} \int_{\Lambda} \boldsymbol{\omega}(\mathbf{x}') \times \frac{\mathbf{x} - \mathbf{x}'}{|\mathbf{x} - \mathbf{x}'|^3} d^3\mathbf{x}', \quad (3)$$

where the integration domain Λ is taken to be infinite or periodic. In index notation (3) becomes

$$u_i(\mathbf{x}) = \frac{1}{4\pi} \int_{\Lambda} \epsilon_{ilk} \omega_l(\mathbf{x}') \frac{(x_k - x'_k)}{|\mathbf{x} - \mathbf{x}'|^3} d^3\mathbf{x}', \quad (4)$$

where ϵ_{ilk} is the cyclic permutation tensor. The derivative with respect to x_j gives the velocity gradient tensor

$$\frac{\partial}{\partial x_j} u_i(\mathbf{x}) = \frac{1}{4\pi} \int_{\Lambda} \epsilon_{ilk} \omega_l(\mathbf{x}') \left[\frac{\delta_{kj}}{r^3} - 3 \frac{r_k r_j}{r^5} \right] d^3\mathbf{x}', \quad (5)$$

where $r \equiv |\mathbf{x} - \mathbf{x}'|$ and $r_m \equiv x_m - x'_m$. The strain rate tensor S_{ij} at \mathbf{x} is the symmetric part of the velocity gradient, namely

$$S_{ij}(\mathbf{x}) \equiv \frac{1}{2} \left(\frac{\partial u_i}{\partial x_j} + \frac{\partial u_j}{\partial x_i} \right). \quad (6)$$

From (5) and (6), $S_{ij}(\mathbf{x})$ can be expressed [15] as an integral over the vorticity field as

$$S_{ij}(\mathbf{x}) = \frac{3}{8\pi} \int_{\Lambda} (\epsilon_{ikl} r_j + r_i \epsilon_{jkl}) \frac{r_k}{r^5} \omega_l(\mathbf{x}') d^3\mathbf{x}'. \quad (7)$$

As shown in Fig. 1, the total strain rate in (7) is separated into the local contribution induced by the vorticity within a spherical region of radius R centered on the point \mathbf{x} and the remaining nonlocal (background) contribution induced by all the vorticity outside this spherical region. The strain rate tensor in (7) thus becomes

$$S_{ij}(\mathbf{x}) = \underbrace{\frac{3}{8\pi} \int_{r \leq R} [\dots] d^3\mathbf{x}'}_{\equiv S_{ij}^R(\mathbf{x})} + \underbrace{\frac{3}{8\pi} \int_{r > R} [\dots] d^3\mathbf{x}'}_{\equiv S_{ij}^B(\mathbf{x})}, \quad (8)$$

where $[\dots]$ denotes the integrand in (7). The nonlocal background strain tensor at \mathbf{x} is then

$$S_{ij}^B(\mathbf{x}) = S_{ij}(\mathbf{x}) - S_{ij}^R(\mathbf{x}). \quad (9)$$

The total strain tensor $S_{ij}(\mathbf{x})$ in (9) is readily evaluated via (6) from derivatives of the velocity field at point \mathbf{x} . Thus all that is required to obtain the background (nonlocal) strain rate tensor $S_{ij}^B(\mathbf{x})$ via (9) is an evaluation of the local strain integral $S_{ij}^R(\mathbf{x})$ in (8) produced by the vorticity field $\omega_l(\mathbf{x}')$ within $r \leq R$ in Fig. 1.

A. Evaluating the Background Strain Rate Tensor

The vorticity field within the sphere of radius R can be represented by its Taylor expansion about the center point \mathbf{x} as

$$\begin{aligned} \omega_l(\mathbf{x}')|_{r \leq R} &= \omega_l(\mathbf{x}) + (x'_m - x_m) \frac{\partial \omega_l}{\partial x_m} \Big|_{\mathbf{x}} \\ &+ \frac{1}{2} (x'_m - x_m) (x'_n - x_n) \frac{\partial^2 \omega_l}{\partial x_m \partial x_n} \Big|_{\mathbf{x}} + \dots \end{aligned} \quad (10)$$

Recalling that $x_m - x'_m \equiv r_m$ and using $a_l, b_{lm}, c_{lmn}, \dots$ to abbreviate the vorticity and its derivatives at \mathbf{x} , we can write (10) as

$$\omega_l(\mathbf{x}')|_{r \leq R} \equiv a_l - r_m b_{lm} + \frac{1}{2} r_m r_n c_{lmn} - \dots \quad (11)$$

Substituting (11) in the S_{ij}^R integral in (8) and changing the integration variable to $\mathbf{r} = \mathbf{x} - \mathbf{x}'$, the strain tensor at \mathbf{x} produced by the vorticity in R is

$$\begin{aligned} S_{ij}^R(\mathbf{x}) &= \frac{3}{8\pi} \int_{r \leq R} (\epsilon_{ikl} r_j + r_i \epsilon_{jkl}) \frac{r_k}{r^5} \\ &\times \left[a_l - r_m b_{lm} + \frac{r_m r_n}{2} c_{lmn} - \dots \right] d^3\mathbf{r}. \end{aligned} \quad (12)$$

This integral can be solved in spherical coordinates centered on \mathbf{x} , with $r_1 = r \sin \theta \cos \phi$, $r_2 = r \sin \theta \sin \phi$, and

$r_3 = r \cos \theta$ for $r \in [0, R]$, $\theta \in [0, \pi]$, and $\phi \in [0, 2\pi)$. To integrate (12) note that

$$\int_{r \leq R} \frac{r_k r_j}{r^5} d^3 \mathbf{r} = \frac{4\pi}{3} \delta_{jk} \int_0^R \frac{1}{r} dr, \quad (13a)$$

$$\int_{r \leq R} \frac{r_k r_j r_m}{r^5} d^3 \mathbf{r} = 0, \quad (13b)$$

$$\int_{r \leq R} \frac{r_k r_j r_m r_n}{r^5} d^3 \mathbf{r} = \frac{2\pi}{15} R^2 (\delta_{mn} \delta_{jk} + \delta_{mj} \delta_{kn} + \delta_{mk} \delta_{jn}). \quad (13c)$$

The resulting local strain rate tensor at \mathbf{x} is then

$$S_{ij}^R(\mathbf{x}) = \frac{R^2}{40} c_{lmn} (\epsilon_{ijl} \delta_{mn} + \epsilon_{jil} \delta_{mn} + \epsilon_{inl} \delta_{mj} + \epsilon_{jnl} \delta_{mi} + \epsilon_{iml} \delta_{nj} + \epsilon_{jml} \delta_{ni}) + O(R^4), \quad (14)$$

where the contribution from the a_l term in (12) is zero since $\epsilon_{ijl} = -\epsilon_{jil}$. For the same reason the first two terms in (14) also cancel, giving

$$S_{ij}^R(\mathbf{x}) = \frac{R^2}{40} c_{lmn} (\epsilon_{inl} \delta_{mj} + \epsilon_{jnl} \delta_{mi} + \epsilon_{iml} \delta_{nj} + \epsilon_{jml} \delta_{ni}) + O(R^4). \quad (15)$$

Recalling that $c_{lmn} = c_{lnm} \equiv \partial^2 \omega_l / \partial x_m \partial x_n$, and contracting with the δ and ϵ in (15), gives

$$S_{ij}^R(\mathbf{x}) = \frac{R^2}{20} \left[\frac{\partial}{\partial x_j} \left(\epsilon_{iml} \frac{\partial \omega_l}{\partial x_m} \right) + \frac{\partial}{\partial x_i} \left(\epsilon_{jml} \frac{\partial \omega_l}{\partial x_m} \right) \right] + O(R^4). \quad (16)$$

Note that $\epsilon_{iml} \partial \omega_l / \partial x_m \equiv (\nabla \times \boldsymbol{\omega})_i$ and

$$\nabla \times \boldsymbol{\omega} = \nabla \times (\nabla \times \mathbf{u}) = \nabla (\nabla \cdot \mathbf{u}) - \nabla^2 \mathbf{u}, \quad (17)$$

so for an incompressible flow ($\nabla \cdot \mathbf{u} \equiv 0$) the local strain rate tensor at \mathbf{x} becomes

$$S_{ij}^R(\mathbf{x}) = -\frac{R^2}{20} \nabla^2 \left(\frac{\partial u_i}{\partial x_j} + \frac{\partial u_j}{\partial x_i} \right) + O(R^4). \quad (18)$$

From (9), with S_{ij}^R from (18) we obtain the background strain tensor as

$$S_{ij}^B(\mathbf{x}) = S_{ij}(\mathbf{x}) + \frac{R^2}{10} \nabla^2 S_{ij}(\mathbf{x}) + O(R^4). \quad (19)$$

The remaining terms in (19) result from the higher-order terms in (11). The contributions from each of these can be evaluated in an analogous manner, giving

$$S_{ij}^B(\mathbf{x}) = \left[1 + \frac{R^2}{10} \nabla^2 + \frac{R^4}{280} \nabla^2 \nabla^2 + \dots + \frac{3R^{2n-2}}{(2n-2)!(4n^2-1)} (\nabla^2)^{n-1} + \dots \right] S_{ij}(\mathbf{x}), \quad (20)$$

where the terms shown in (20) correspond to $n = 1, 2, \dots$. The final result in (20) is an operator that extracts the nonlocal background strain rate tensor S_{ij}^B at any point \mathbf{x} from the total strain rate tensor S_{ij} . For the Taylor expansion in (10), this operator involves Laplacians of the total strain rate field $S_{ij}(\mathbf{x})$.

B. Practical Implementation

When using (20) to examine the local alignment of any concentrated vortical structure with the principal axes of the background strain rate field $S_{ij}^B(\mathbf{x})$ in which it resides, the radius R must be taken sufficiently large that the spherical region $|\mathbf{x}' - \mathbf{x}| \leq R$ encloses essentially all the vorticity associated with the structure, so that its local induced strain rate field is fully accounted for. Generally, as R increases it is necessary in (20) to retain terms of increasingly higher order n to maintain a sufficient representation of $\boldsymbol{\omega}(\mathbf{x}')$ over the spherical region. Thus for any vortical structure having a characteristic gradient lengthscale λ_ν , it can be expected that R must be of the order of λ_ν , and n will then need to be sufficiently large to adequately represent the vorticity field within this sphere. However, since the local gradient lengthscale in the vorticity field in a turbulent flow is determined by an equilibrium between strain and diffusion, the vorticity field over the lengthscale λ_ν will be relatively smooth, and thus relatively low values of n may suffice to give a usable representation of $\boldsymbol{\omega}(\mathbf{x}')$. This is examined in the following Section.

III. TEST CASE: BURGERS VORTEX

The equilibrium Burgers vortex [1, 3, 9, 16] is formed from vorticity in a fluid with viscosity ν by a spatially uniform, irrotational, axisymmetric background strain rate field S_{ij}^B that has a single extensional principal strain rate S_{zz} directed along the z axis, as shown in Fig. 2. This simple flow, often regarded as an idealized model of the most concentrated vortical structures in turbulent flows, provides a test case for the result in (20). The combined strain rate field $S_{ij}(\mathbf{x})$ produced by the vortex and the background strain flow should, when applied

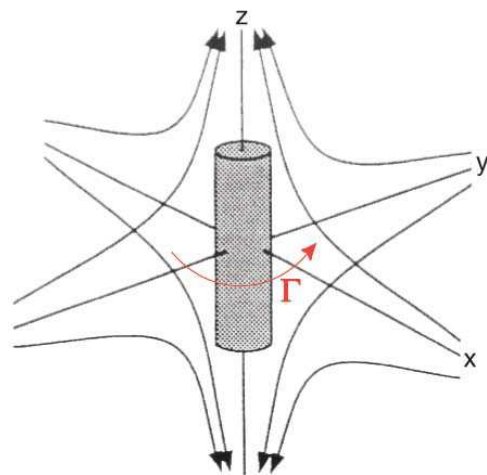


FIG. 2: Equilibrium Burgers vortex with circulation Γ and strain-limited viscous diffusion lengthscale λ_ν in a uniform, irrotational, axisymmetric background strain rate field $S_{ij}^B(\mathbf{x})$.

in (20), produce the underlying background strain field $(S_{rr}^B, S_{\theta\theta}^B, S_{zz}^B) = (-\frac{1}{2}, -\frac{1}{2}, 1)S_{zz}$ at all \mathbf{x} when $R \rightarrow \infty$ and all orders n are retained. For finite R and n , the resulting $S_{ij}^B(\mathbf{x})$ will reflect the convergence properties of (20).

A. Strain Rate Tensor

The equilibrium Burgers vortex aligned with the extensional principal axis of the background strain rate field has a vorticity field

$$\boldsymbol{\omega}(\mathbf{x}) = \omega_z(r)\hat{\mathbf{z}} = \frac{\alpha}{\pi} \frac{\Gamma}{\lambda_\nu^2} \exp(-\alpha\eta^2) \hat{\mathbf{z}}, \quad (21)$$

where Γ is the circulation, λ_ν is the viscous lengthscale that characterizes the diameter of the vortex, $\eta \equiv r/\lambda_\nu$ is the radial similarity coordinate, and the constant α reflects the chosen definition of λ_ν . Following [9], λ_ν is taken as the full width of the vortical structure at which ω_z has decreased to one-fifth of its peak value, for which $\alpha = 4 \ln 5$. When diffusion of the vorticity is in equilibrium [9] with the background strain, then

$$\lambda_\nu = \sqrt{8\alpha} \left(\frac{\nu}{S_{zz}} \right)^{1/2}. \quad (22)$$

The combined velocity field $\mathbf{u}(\mathbf{x})$ produced by the vortex and the irrotational background strain is given by the cylindrical components

$$u_r(r, \theta, z) = -\frac{S_{zz}}{2} r, \quad (23a)$$

$$u_\theta(r, \theta, z) = \frac{\Gamma}{2\pi\lambda_\nu} \frac{1}{\eta} [1 - \exp(-\alpha\eta^2)], \quad (23b)$$

$$u_z(r, \theta, z) = S_{zz} z. \quad (23c)$$

The combined strain rate tensor for such a Burgers vortex is thus

$$S_{ij}(\mathbf{x}) = \begin{bmatrix} -S_{zz}/2 & S_{r\theta}^v & 0 \\ S_{r\theta}^v & -S_{zz}/2 & 0 \\ 0 & 0 & S_{zz} \end{bmatrix}, \quad (24)$$

where $S_{r\theta}^v$ is the shear strain rate induced by the vortex, given by

$$S_{r\theta}^v(\mathbf{x}) = \frac{\Gamma}{\pi\lambda_\nu^2} \left[\left(\alpha + \frac{1}{\eta^2} \right) \exp(-\alpha\eta^2) - \frac{1}{\eta^2} \right]. \quad (25)$$

From (24), $S_{ij}(\mathbf{x})$ has one extensional principal strain rate equal to S_{zz} along the $\hat{\mathbf{z}}$ axis, with the remaining two principal strain axes lying in the r - θ plane and corresponding to the principal strain rates

$$s = -\frac{1}{2}S_{zz} \pm |S_{r\theta}^v|. \quad (26)$$

As long as the largest s in (26) is smaller than S_{zz} , the most extensional principal strain rate s_1 of S_{ij} will be

S_{zz} , and the corresponding principal strain axis will point in the $\hat{\mathbf{z}}$ direction. The vorticity is then aligned with the most extensional eigenvector of S_{ij} . This remains the case until the vortex becomes sufficiently strong relative to the background strain rate that $s > S_{zz}$, namely

$$|S_{r\theta}^v| \geq \frac{3}{2}S_{zz}, \quad (27)$$

which from (25) occurs wherever

$$\left(\alpha + \frac{1}{\eta^2} \right) \exp(-\alpha\eta^2) - \frac{1}{\eta^2} \geq \frac{3\pi}{2} \left(\frac{\Gamma/\lambda_\nu^2}{S_{zz}} \right)^{-1}. \quad (28)$$

At any η for which (28) is satisfied, the most extensional principal axis of the combined strain rate tensor $S_{ij}(\mathbf{x})$ will switch from the $\hat{\mathbf{z}}$ direction to instead lie in the r - θ plane. Since the vorticity vector everywhere points in the $\hat{\mathbf{z}}$ direction, wherever (28) is satisfied the principal axis of S_{ij} that is aligned with the vorticity will switch from the most extensional eigenvector to the intermediate eigenvector. This alignment switching is purely a result of the induced strain field $S_{ij}^v(\mathbf{x})$ locally dominating the background strain field $S_{ij}^B(\mathbf{x})$.

The dimensionless vortex strength parameter

$$\Omega \equiv \left[\frac{\Gamma/\lambda_\nu^2}{S_{zz}} \right] = \frac{\pi \omega_{max}}{\alpha S_{zz}} \quad (29)$$

on the right-hand side of (28) characterizes the relative strength of the background strain and the induced strain from the vortical structure, where ω_{max} is obtained from (21) at $\eta = 0$. For

$$\Omega < \Omega^* \approx 2.45, \quad (30)$$

the background strain rate S_{zz} is everywhere larger than the largest s in (26), and thus no alignment switching occurs at any η . For $\Omega > \Omega^*$, alignment switching will occur over the limited range of η values that satisfy (28). With increasing values of Ω , more of the vorticity field will be aligned with the intermediate principal axis of the *combined* strain rate tensor, even though all of the vorticity field remains aligned with the most extensional principal axis of the *background* strain rate tensor.

Figure 3 shows the vorticity ω_z and the induced shear strain component $-S_{r\theta}^v$ as a function of η . The horizontal dashed lines correspond to three different values of Ω , and indicate the range of η values where the alignment switching in (28) occurs for each Ω . Wherever $-S_{r\theta}^v$ is above the dashed line for a given Ω , the vorticity will be aligned with the local intermediate principal axis of the combined strain rate field.

In principle, regardless of the vortex strength parameter Ω , at any η the result in (20) can reveal the alignment of the vorticity with the most extensional principal axis of the background strain field S_{ij}^B . However, this requires R to be sufficiently large that a sphere with diameter $2R$, centered at the largest η for which $-S_{r\theta}^v$ in Fig. 3 is still

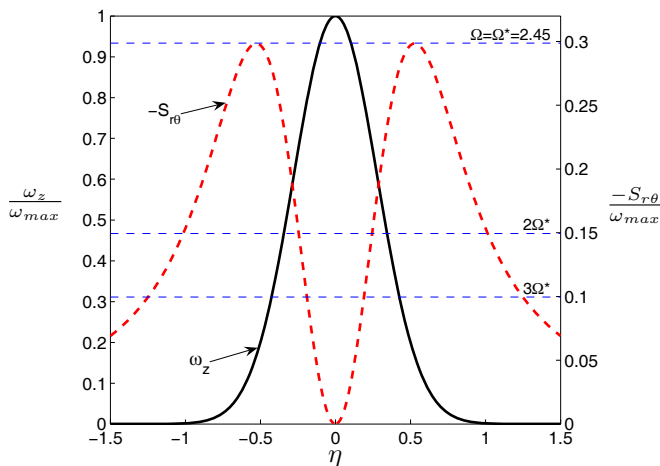


FIG. 3: Similarity profiles of $\omega_z(\eta)$ and $S_{r\theta}(\eta)$ for any equilibrium Burgers vortex; wherever $-S_{r\theta}$ exceeds the horizontal line determined by the relative vortex strength parameter Ω in (29) the most extensional principal axis of the total strain rate $S_{ij}(\mathbf{x})$ switches from the $\hat{\mathbf{z}}$ -axis to lie in the r - θ plane.

above the horizontal dashed line, will enclose essentially all of the vorticity associated with the vortical structure. As Ω increases, the required R will increase accordingly as dictated by (28), and as R is increased the required n in (20) also increases.

Irrespective of the value of Ω , when (20) is applied to the combined strain rate field $S_{ij}(\mathbf{x})$ in (24) and (25), if $\tilde{R} \equiv (R/\lambda_\nu) \rightarrow \infty$ and all orders n are retained then the resulting $S_{ij}^B(\mathbf{x})$ should recover the background strain field, namely

$$S_{r\theta}^B \rightarrow 0 \quad (31)$$

for all \mathbf{x} , and the vorticity should show alignment with the most extensional principal axis of S_{ij}^B . For finite R/λ_ν and various orders n , the convergence of S_{ij}^B from (20) to this background strain field is examined below.

B. Convergence of the Background Strain

The accuracy with which (20) can recover the background strain field $S_{ij}^B(\mathbf{x})$ that acts on a concentrated vortical structure depends on how well the expansion in (10) represents the vorticity field within the local spherical neighborhood R . Figure 4 shows the results of a local sixth-order Taylor series approximation for the vorticity in (21) at various radial locations across the Burgers vortex. In each panel, the blue square marks the location \mathbf{x} at which the sphere is centered, and the red dashed curve shows the resulting Taylor series approximation for the vorticity. On the axis of the vortex, the approximated vorticity field correctly accounts for most of the circulation in the vortex, and thus the induced strain field from the vortex will be reasonably approximated. Off the axis,

the approximation becomes increasingly poorer, but the $1/r^2$ decrease in the Biot-Savart kernel in (3) nevertheless renders it adequate to account for most of the vortex-induced strain rate field. At the largest radial location, corresponding to the bottom right panel of Fig. 4, the approximation becomes relatively poor, however at large η values the vortex-induced strain is sufficiently small that it is unlikely to lead to alignment switching for typical Ω values.

Figure 5 shows the shear component $S_{r\theta}^B(\eta)$ of the background strain rate tensor obtained via (20) for various n and \tilde{R} as a function of η . In each panel, the black curve shows the total strain rate $S_{ij}(\eta)$ and the colored curves show the background strain rate $S_{ij}^B(\eta)$ from (20) for the (n, \tilde{R}) combinations listed. The horizontal dashed line corresponding to $\Omega = (3/2)\Omega^*$ reflects the relative vortex strength, and shows the range of η where the anomalous alignment switching occurs due to the vortex-induced strain field. Wherever the $-S_{r\theta}^B$ curves are above this line, the vorticity there will be aligned with the intermediate principal axis of the *combined* strain rate tensor S_{ij} . Figure 5(a) examines the effect of increasing the radius \tilde{R} of the spherical region for fixed order $n = 6$. It is apparent that with increasing \tilde{R} the resulting $-S_{r\theta}^B$ converges toward the correct background strain field in (31). For the value of Ω shown, it can be seen that for $R \gtrsim 0.5\lambda_\nu$ the resulting $S_{r\theta}^B$ is everywhere below the horizontal dashed line, indicating that the vorticity everywhere is aligned with the most extensional principal axis of the resulting background strain rate tensor $S_{ij}^B(\mathbf{x})$ from (20).

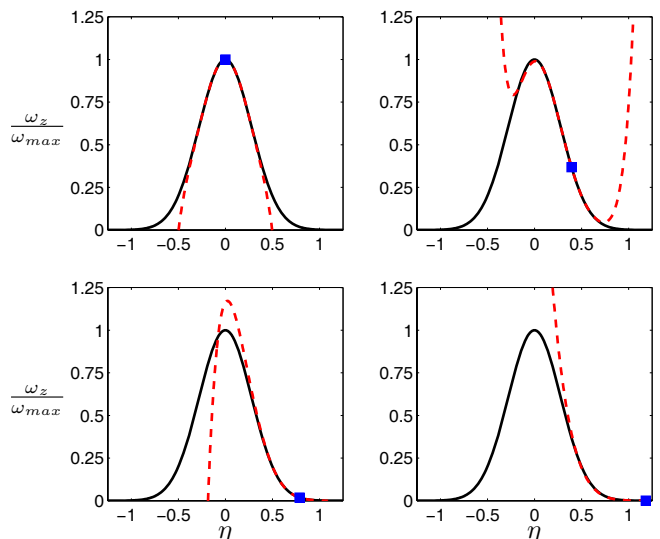


FIG. 4: Accuracy of the Taylor expansion for the local vorticity in (10) for a Burgers vortex, showing results for 6th order approximation. In each panel, solid black curve shows actual vorticity profile, and red dashed curve gives approximated vorticity from derivatives at location marked by square.

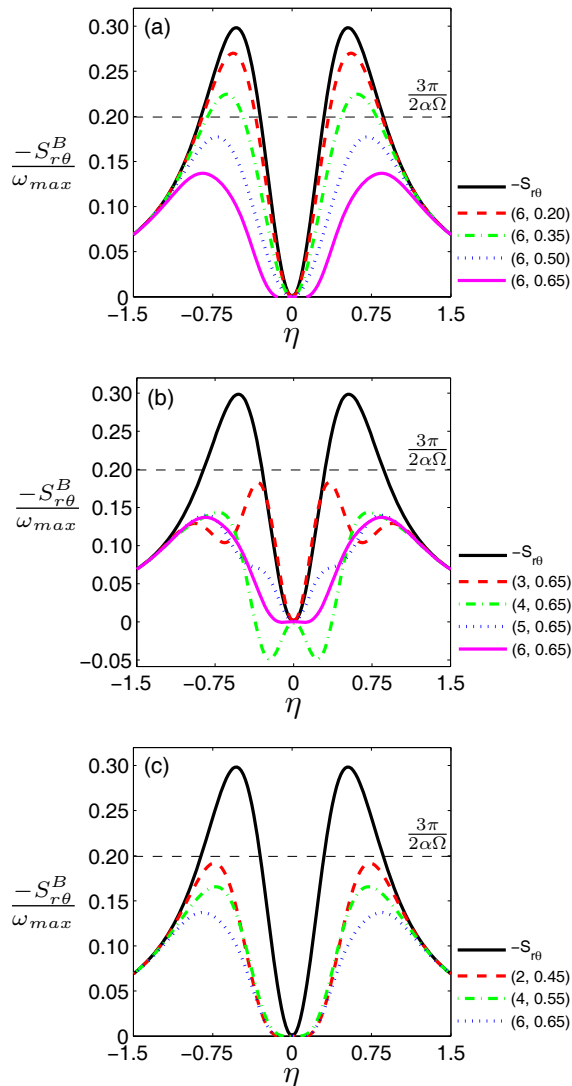


FIG. 5: Convergence of background strain rate field $S_{ij}^B(\mathbf{x})$ for a Burgers vortex, obtained from total strain rate field $S_{ij}(\mathbf{x})$ using (20) for various (n, \tilde{R}) combinations, where $\tilde{R} \equiv R/\lambda_\nu$. Shown are effects of increasing \tilde{R} for fixed $n = 6$ (top), increasing n for fixed $\tilde{R} = 0.65$ (middle), and increasing n and \tilde{R} simultaneously (bottom). The dashed horizontal lines follow from (27) and (29).

In Fig. 5(b) similar results are shown for the effect of increasing the order n of the expansion for the vorticity field for fixed $\tilde{R} = 0.65$. It is apparent that the effect of n is somewhat smaller than for \tilde{R} in Fig. 5(a). Moreover, the results suggest that the series in (20) alternates with increasing order n . For this Ω and \tilde{R} , even $n = 3$ is seen to be sufficient to remove most of the vortex-induced shear strain, and thus reduce $S_{r\theta}^B(\mathbf{x})$ below the horizontal dashed line. For these parameters, the $S_{r\theta}^B$ field from (20) would thus reveal alignment of the vorticity with the

most extensional principal axis of the background strain tensor throughout the entire field.

Figure 5(c) shows the combined effects of increasing both \tilde{R} and n , in accordance with the expectation that larger \tilde{R} should require a higher order n to adequately represent the vorticity field within the spherical region. The shear strain rate field shows convergence to the correct background strain field in (31). The convergence of the shear strain rate $S_{r\theta}^B(\mathbf{x})$ to zero in the vicinity of the vortex core is of particular importance. The systematic reduction in the peak remaining shear stress indicates that, even for increasingly stronger vortices or increasingly weaker background strain fields as measured by Ω , the resulting $S_{r\theta}^B(\mathbf{x})$ from (20) will reveal the alignment of all the vorticity in such a structure with the most extensional principal strain axis of the background strain field.

IV. VORTICITY ALIGNMENT IN TURBULENT FLOWS

Having seen in the previous Section how (20) is able to reveal the expected alignment of vortical structures with the most extensional eigenvector of the *background* strain rate in which they reside, in this Section we apply it to obtain insights into the vorticity alignment in turbulent flows. In particular, we examine the alignment at every point \mathbf{x} of the vorticity $\boldsymbol{\omega}$ relative to the eigenvectors of the total strain rate tensor field $S_{ij}(\mathbf{x})$ and those of the background strain field data $S_{ij}^B(\mathbf{x})$. This analysis uses data from a highly-resolved, three-dimensional, direct numerical simulation (DNS) of statistically stationary, forced, homogeneous, isotropic turbulence [17, 18]. The simulations correspond to a periodic cube with sides of length of 2π resolved by 2048^3 grid points. The Taylor microscale Reynolds number R_λ is 107.

The DNS data were generated by a pseudospectral method with a spectral resolution that exceeds the standard value by a factor of eight. As a result, the highest wavenumber corresponds to $k_{max}\eta_K = 10$, and the Kolmogorov lengthscale $\eta_K = \nu^{3/4}/\langle\epsilon\rangle^{1/4}$ is resolved with three grid spacings. This superfine resolution makes it possible to apply the result in (20) for relatively high orders n , which require accurate evaluation of high-order derivatives of the DNS data. In Schumacher *et al.* [17] it was demonstrated that derivatives up to order six are statistically converged. More details on the numerical simulations are given in Refs. [17, 18].

Figure 6 gives a representative sample of the DNS data, where the instantaneous shear component S_{12} of the total strain rate tensor field $S_{ij}(\mathbf{x})$ is shown in a typical two-dimensional intersection through the 2048^3 cube. The data can be seen to span nearly $700\eta_K$ in each direction. The 512^2 box at the lower left of Fig. 6 is used here to obtain initial results for alignment of the vorticity with the eigenvectors of the background strain rate tensor.

The background strain rate tensor field $S_{ij}^B(\mathbf{x})$ is first

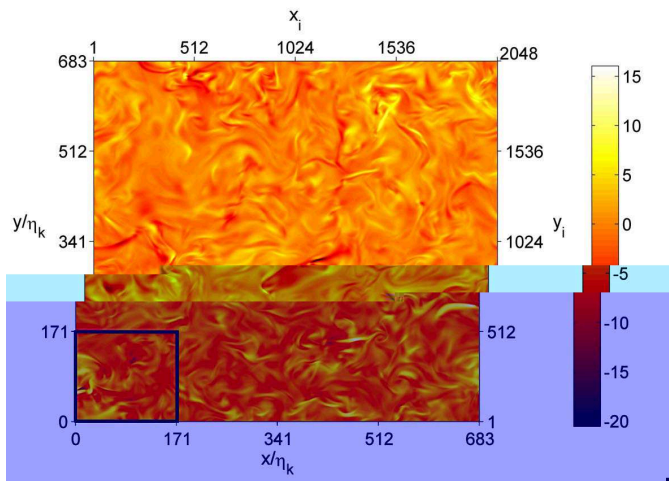


FIG. 6: Instantaneous snapshot of total strain rate component field $S_{12}(\mathbf{x})$ in a two-dimensional slice through a highly-resolved three-dimensional (2048^3) DNS of homogeneous, isotropic turbulence [17, 18]. Axes are given both in grid coordinates ($i = 1 \dots 2048$) and normalized by the Kolmogorov length η_K . Box indicates region in which background strain rate field $S_{ij}^B(\mathbf{x})$ is computed in Fig. 7.

extracted via (20) from $S_{ij}(\mathbf{x})$ for $n = 3$ and various (R/η_K) . Higher-order evaluation of the background strain rate is not feasible, as the results in Ref. [17] show that only spatial derivatives of the velocity field up to order six can be accurately obtained from these high-resolution DNS data. For $n = 4$, the expansion in (20) involves seventh-order derivatives of the velocity field, and the background strain evaluation becomes limited due to the grid resolution. The results are shown and compared in Fig. 7, where the shear component S_{12} of the full strain rate tensor is shown at the top, and the corresponding nonlocal (background) component S_{12}^B and local component S_{12}^R are shown, respectively, in the left and right columns for $(R/\eta_K) = 2.5$ (top row), 3.5 (middle row), and 4.5 (bottom row). Consistent with the results from the Burgers vortex in Fig. 5, as (R/η_K) increases the magnitude of the extracted local strain rate in the right column increases. However, for the largest $(R/\eta_K) = 4.5$ case, $n = 3$ appears to be too small to adequately represent the local vorticity field. This leads to truncation errors which are manifested as strong ripples in the background and local strain fields (see panels (f) and (g)).

The results in Fig. 7 thus indicate that radii up to $(R/\eta_K) = 3.5$ in combination with $n = 3$ can be used to assess alignment of the vorticity vector with the eigenvectors of the background strain rate field. Figure 8 shows the probability densities of the alignment cosines for the vorticity vector with the total strain rate tensor and with the background strain rate tensors from (20). We compare S_{ij} (Fig. 8a) with S_{ij}^B for $(R/\eta_K) = 2.5, n = 3$ (Fig. 8b) and S_{ij}^B for $(R/\eta_K) = 3.5, n = 3$ (Fig. 8c). The results for alignment with the total strain rate tensor are essentially identical to the anomalous alignment seen in

numerous other DNS studies [5, 6, 7] and experimental studies [8, 9, 10, 11, 12], which show the vorticity to be predominantly aligned with the eigenvector corresponding to the intermediate principal strain rate. However, the results for the Burgers vortex in the previous section show that such anomalous alignment with the eigenvectors of the total strain rate tensor is expected when the local vortex strength parameter Ω is sufficiently large to cause alignment switching.

By comparison, the results in Fig. 8 (b) and (c) obtained for the alignment cosines of the vorticity vector with the *background* strain rate tensor S_{ij}^B from (20) show a significant decrease in alignment with the intermediate eigenvector, and an increase in alignment with the most extensional eigenvector. While data in panel (b) show only a slight change compared to those in (a), the results in panel (c) demonstrate that our decomposition can indeed diminish the anomalous alignment signif-

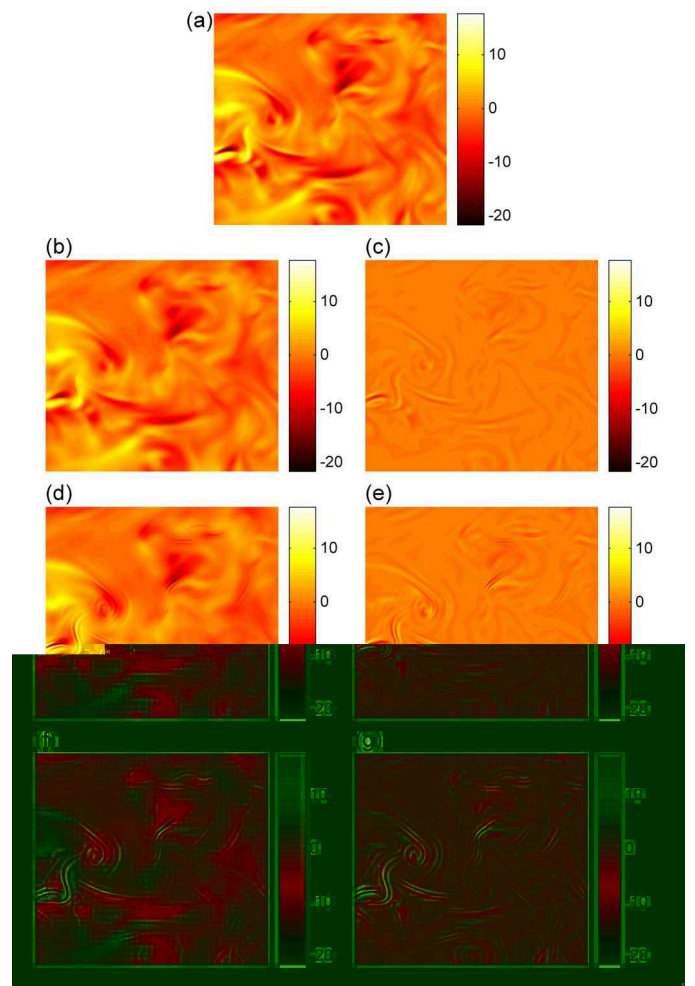


FIG. 7: Total strain rate component field $S_{12}(\mathbf{x})$ (a), with corresponding results from (20) for nonlocal (background) field $S_{12}^B(\mathbf{x})$ (left) and local field $S_{12}^R(\mathbf{x})$ (right) for $(R/\eta_K) = 2.5$ (b, c), $(R/\eta_K) = 3.5$ (d, e), and $(R/\eta_K) = 4.5$ (f, g), all with $n = 3$.

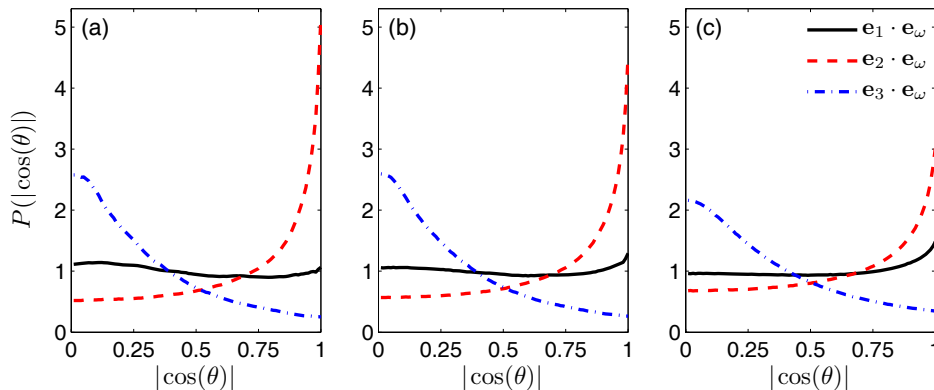


FIG. 8: Probability densities of alignment cosines for the vorticity with the eigenvectors of the strain rate tensor, showing results for S_{ij}^R (a) and for S_{ij}^B using $(R/\eta_K) = 2.5$ with $n = 3$ (b) and $(R/\eta_K) = 3.5$ with $n = 3$ (c).

icantly. This is consistent with the results for the Burgers vortex in the previous Section, and with the hypothesis that the alignment switching mechanism due to the local contribution S_{ij}^R to the total strain rate tensor is the primary reason for the anomalous alignment seen in earlier studies. It is also consistent with the expected equilibrium alignment from (1). While a more detailed study is needed to examine possible nonequilibrium contributions to the alignment distributions associated with eigenvector rotations of the background strain field, as well as to definitively determine the R and n convergence of the background strain rate tensor in Fig. 7, the present findings support both the validity of the result in (20) for extracting the background strain rate tensor field $S_{ij}^B(\mathbf{x})$ from the total strain rate tensor field $S_{ij}(\mathbf{x})$, and the hypothesis that at least much of the anomalous alignment of vorticity in turbulent flows is due to the differences between the total and background strain rate tensors and the resulting alignment switching noted herein.

V. CONCLUDING REMARKS

We have developed a systematic and exact result in (20) that allows the local and nonlocal (background) contributions to the total strain rate tensor S_{ij} at any point \mathbf{x} in a flow to be disentangled. The approach is based on a series expansion of the vorticity field in a local spherical neighborhood of radius R centered at the point \mathbf{x} . This allows the background strain rate tensor field $S_{ij}^B(\mathbf{x})$ to be determined via a series of increasingly higher-order Laplacians applied to the total strain rate tensor field $S_{ij}(\mathbf{x})$. For the Burgers vortex, with increasing radius R relative to the local gradient lengthscale λ_ν and with increasing order n , we demonstrated convergence of the resulting background strain tensor field to its theoretical form. We also showed that even with limited R and n values, the local contribution to the total strain rate tensor field can be sufficiently removed to eliminate the

anomalous alignment switching throughout the flow field. This conclusion is expected to also apply to the more realistic case of a non-uniformly stretched vortex where $S_{zz} = f(z)$ [16, 19, 20, 21].

Consistent with the results for the Burgers vortex, when (20) was used to determine the background strain rate tensor field $S_{ij}^B(\mathbf{x})$ in highly-resolved DNS data for a turbulent flow, the anomalous alignment seen in previous DNS and experimental studies was substantially reduced. We conclude that (20) allows the local background strain rate tensor to be determined in any flow. Furthermore, we postulate that the vorticity vector field in turbulent flows will show a substantially preferred alignment with the most extensional principal axis of the background strain rate field, and that at least much of the anomalous alignment found in previous studies is simply a reflection of the alignment switching mechanism analyzed in Section III and conjectured by numerous previous investigators.

Lastly, the result in (20) is based on a Taylor series expansion of the vorticity within a spherical neighborhood of radius R around any point \mathbf{x} . Such an expansion inherently involves derivatives of the total strain rate tensor field, which can lead to potential numerical limitations. If larger R and correspondingly higher orders n are needed to obtain accurate evaluations of background strain rate fields, then otherwise identical approaches based on alternative expansions may be numerically advantageous. For instance, an expansion in terms of orthonormal basis functions allows the coefficients to be expressed as integrals over the vorticity field within $r \leq R$, rather than as derivatives evaluated at the center point \mathbf{x} . (For example, wavelets have been used to test alignment between the strain rate eigenvectors and the vorticity gradient in two-dimensional turbulence [22].) This would allow a result analogous to (20) that can be carried to higher orders with less sensitivity to discretization error. The key conclusion, however, of the present study is that it is possible to evaluate the background strain tensor following the

general procedure developed herein, and that when such methods are applied to assess the background strain rate fields in turbulent flows they reveal a substantial increase in the expected alignment of the vorticity vector with the most extensional principal axis of the background strain rate field.

Acknowledgments

PH and WD acknowledge support from the Air Force Research Laboratory (AFRL) under the Michigan AFRL Collaborative Center for Aeronautical Sciences (MAC-

CAS), and by the National Aeronautics & Space Administration (NASA) Marshall and Glenn Research Centers and the Department of Defense (DoD) under the NASA Constellation University Institutes Project (CUIP) under Grant No. NCC3-989. JS acknowledges support by the German Academic Exchange Service (DAAD) and by the Deutsche Forschungsgemeinschaft (DFG) under grant SCHU 1410/2. The direct numerical simulations have been carried out within the Deep Computing Initiative of the DEISA consortium on 512 CPUs of the IBM-p690 cluster JUMP at the John von Neumann Institute for Computing at the Research Centre Jülich (Germany).

-
- [1] J. M. Burgers, *Adv. Appl. Mech.* **1**, 171 (1948).
 - [2] G. K. Batchelor, *J. Fluid Mech.* **20**, 640 (1964).
 - [3] T. S. Lundgren, *Phys. Fluids* **25**, 2193 (1982).
 - [4] T. S. Lundgren, *Phys. Fluids A5*, 1472 (1993).
 - [5] Wm. T. Ashurst, A. R. Kerstein, R. M. Kerr, and C. H. Gibson, *Phys. Fluids* **30**, 2343 (1987).
 - [6] Z.-S. She, E. Jackson, and S. A. Orszag, *Proc. R. Soc. Lond. A* **434**, 101 (1991).
 - [7] K. K. Nomura and G. K. Post, *J. Fluid Mech.* **377**, 65 (1998).
 - [8] A. Tsinober, E. Kit, and T. Dracos, *J. Fluid Mech.* **242**, 169 (1992).
 - [9] K. A. Buch and W. J. A. Dahm, *J. Fluid Mech.* **317**, 21 (1996).
 - [10] L. K. Su and W. J. A. Dahm, *Phys. Fluids* **8**, 1883 (1996).
 - [11] B. W. Zeff, D. D. Lanterman, R. McAllister, R. Roy, E. J. Kostelich, and D. P. Lathrop, *Nature* **421**, 146 (2003).
 - [12] J. A. Mullin and W. J. A. Dahm, *Phys. Fluids* **18**, 035102 (2006).
 - [13] J. Jimenez, *Phys. Fluids A* **4**, 652 (1992).
 - [14] J. G. Brasseur and W. Lin, *Fluid Dyn. Res.* **36**, 357 (2005).
 - [15] K. Ohkitani, *Phys. Rev. E* **50**, 5107 (1994).
 - [16] J. D. Gibbon, A. S. Fokas, and C. R. Doering, *Physica D* **132**, 497 (1999).
 - [17] J. Schumacher, K. R. Sreenivasan, and V. Yakhot, *New J. Phys.* **9**, 89 (2007).
 - [18] J. Schumacher, *Europhys. Lett.* **80**, 54001 (2007).
 - [19] K. Ohkitani, *Phys. Rev. E* **65**, 046304 (2002).
 - [20] Y. Cuypers, A. Maurel, and P. Petitjeans, *Phys. Rev. Lett.* **91**, 194502 (2003).
 - [21] M. Rossi, F. Bottausci, A. Maurel, and P. Petitjeans, *Phys. Rev. Lett.* **92**, 054504 (2004).
 - [22] B. Protas, K. Schneider, and M. Farge, *Phys. Rev. E* **66**, 046307 (2002).